Electronic Supplementary Material (ESI) for Nanoscale.

Supporting document for "Tuning the Hydrogen Evolution Activity of β-Mo_2C Nanoparticles Via Control of Their Growth Conditions"

Timothy T. Yang[1], Wissam A. Saidi [1*]

[1]Department of Materials Science and Engineering, University of Pittsburgh, Pittsburgh, PA 15260, United States

*To whom correspondence should be addressed: alsaidi@pitt.edu

Computational Details

The first-principle calculations are based on density functional theory (DFT) as implemented in the Vienna Ab Initio Simulation Package (VASP). We employ the Perdew-Burke-Ernzerhof (PBE) exchange-correlational functional to solve the Kohn-Sham equations within periodic boundary conditions. The electron-nucleus interactions are described using PAW pseudopotentials.[1,2] The Monkhorst-Pack *k*-point is set to 4 × 4 × 4 for bulk optimization and 4 × 4 × 1 in calculations of slab systems. The partial occupancies of the bands are determined using the first-order scheme of the Methfessel-Paxton method with a 0.05 eV width. We used a planewave cutoff of 400 eV, which was verified to be large enough as using a smaller cutoff of 300 eV changes energy differences by less than 3%. The electronic self-consistent loop is terminated when energy changes are less than 1×10^{-5} eV and the ionic relaxations are considered converged when the magnitude of the largest force on any atom is less than 0.01 eV/Å. Using this computational setup, we find that the optimized hexagonal β-Mo_2C unit cell has dimensions 6.061 × 6.054 × 4.713 $Å^3$, which is in good agreement with previous DFT/RPBE results[3] 6.051 × 6.048 × 4.732 $Å^3$, as well as with experimental results[4] 6.0248 × 6.0248 × 4.7352 $Å^3$.

To determine the equilibrium β-Mo_2C NPs morphology according to Wulff construction scheme, we investigated polar and non-polar polar low Miller index surfaces, which are obtained from bulk using a (1 × 1) surface supercell with 6 atomic layers for non-polar terminations, 18 atomics layers for (100), and 12 for (001) surface. The fictitious interactions between images along the non-periodic direction are mitigated using 10 Å vacuum. We have verified that our results are not sensitive to slab thickness as summarized in Table S2. Further, we show in Table S3 that our hydrogen adsorption Gibbs free energies on (001), (100) and (011) surfaces are in good agreement with previous DFT calculations[5].

The binding energy of (011) surface using two different functionals

We carry out additional calculations for the hydrogen binding energy using RPBE on the (011) surface. Our PBE and RPBE results are shown in the Table 1. As can be seen, the difference between the PBE and RPBE absolute binding energies is small, less than 0.11 eV.

Hydrogen Coverage (H)	PBE (eV)	RPBE (eV)
1	-0.58	-0.47
2	-0.61	-0.50
3	-0.49	-0.38
4	-0.43	-0.32
5	-0.35	-0.24
6	-0.30	-0.19
7	-0.28	-0.17
8	-0.25	-0.14

Table S1

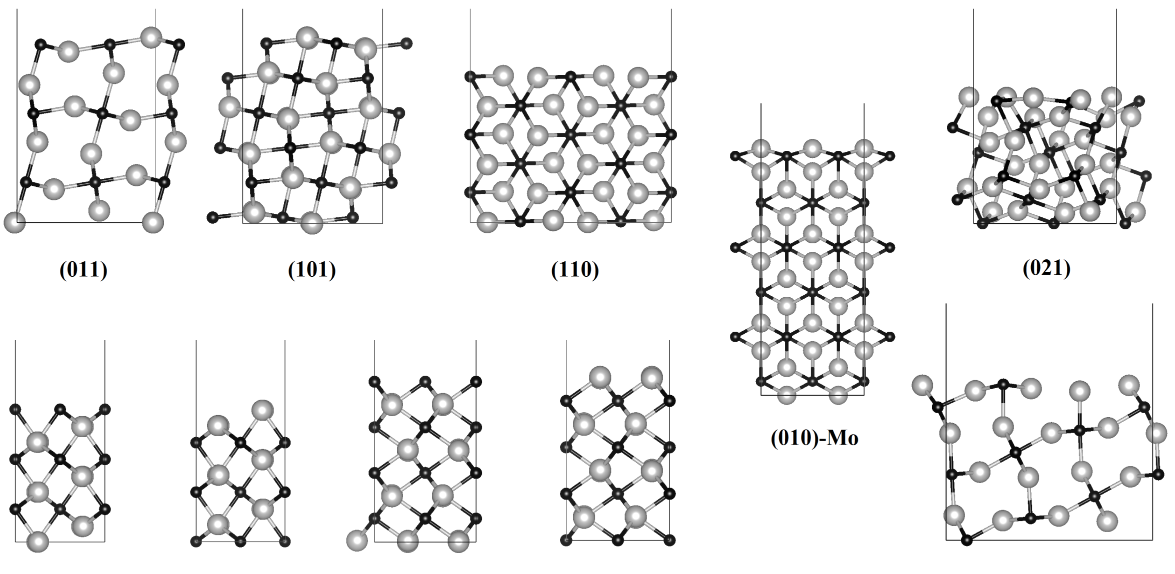
(011) (101) (110) (021) (010)-Mo (100)-C (100)-Mo (001)-C (001)-Mo (111)-Mo

Table S2. The side view of ten β-Mo_2C surfaces. The Molybdenum atoms and the Carbon atoms are in gray and black The number of layer shows on the picture is used in actual DFT calculation.

Table S3. Surface free energies (J/m^2) calculated from 2 layer slabs and 3 layer slabs. Results show the convergence in energies for DFT calculations.

	(011)	(101)	(110)	(021)	(100)-C	(100)-Mo	(001)-C	(001)-Mo	(111)	(010)
2-Layer	3.138	3.116	3.363		3.376	3.396	3.382	3.496		
3-Layer	3.140	3.116	3.375	3.255	3.367	3.390	3.377	3.489	3.255	3.023

Table S4. The comparison of hydrogen adsorption energy (-eV) for four surfaces at hydrogen coverages. The first raw is the reported energies in reference[5], and the second column is the energies calculated in our work.

	1H	2H	3H	4H	5H	6H	7H	8H	9H	10H	11H	12H	13H	14H
(011)	0.650	0.612	0.522	0.470	0.383	0.339								
	0.608	0.628	0.506	0.453	0.373	0.317								
(100)-Mo	0.995	0.998	0.873	0.816	0.677	0.594								
	0.963	0.949	0.870	0.828	0.703	0.613								
(001)-Mo	1.120	1.119	1.011	0.979	0.800									
	1.100	1.113	1.008	0.984	0.765									
(021)	1.020	0.967	0.930	0.919	0.868	0.815	0.741	0.680	0.626	0.595	0.551	0.512	0.482	0.455
	0.989	0.984	0.933	0.949	0.949	0.837	0.762	0.712	0.655	0.637	0.592	0.551	0.521	0.500

Methodology Details

The Helmholtz free energy is defined as,

$$F(T,V) = E_{DFT} + E_{vib} - TS_{vib} \qquad (S1)$$

where the phonon energy E_{vib} and entropy S_{vib} are defined as,

$$E_{vib} = \frac{1}{2}\sum_i h\nu_i + \sum_i \frac{h\nu_i e^{-\frac{h\nu_i}{k_\beta T}}}{1 - e^{-\frac{h\nu_i}{k_\beta T}}} \qquad (S2)$$

$$S_{vib} = k_\beta \sum_i \left(\frac{h\nu_i}{k_\beta T}\right)\frac{e^{-h\nu_i/k_\beta T}}{1 - e^{-h\nu_i/k_\beta T}} - k_\beta \sum_i \ln\left(1 - e^{-\frac{h\nu_i}{k_\beta T}}\right) \qquad (S3)$$

Here ν_i is the phonon frequency, and k_β is Boltzmann constant.

The Gibbs free energy *of H_2 in the gas phase* is defined as

$$G_{\mathrm{H}_2} = E_{\mathrm{H}_2} + \tilde{\mu}_{\mathrm{H}_2}(T,p^0) + k_B T ln\left(\frac{p_{\mathrm{H}_2}}{p^0}\right) \qquad (S4)$$

$$\tilde{\mu}_{\mathrm{H}_2} = [H(T,p^0) - H(0,p^0)] - T[S(T,p^0) - S(0,p^0)] \qquad (S5)$$

We have implied the basic relation in thermodynamics, $G = H - TS$, to express $\tilde{\mu}_{\mathrm{H}_2}$ with enthalpy H and entropy S as a reference to zero temperature at 1 atm. $H(T,p^0)$ and $S(T,p^0)$ for all temperatures are obtained from NIST-JANAF thermochemical tables[6].

The surface free energy and defined as,

$$\gamma_{surf}(T,p) = \frac{1}{2A}\left(G_{slab} - N_{\mathrm{Mo}}\mu_{\mathrm{Mo}} - N_{\mathrm{C}}\mu_{\mathrm{C}}\right) \qquad (S6)$$

where N_i (i=Mo, C) is number of atoms in the system and μ_i is chemical potential, A is the surface area. The slabs are in equilibrium with the bulk which constrains the chemical potentials as $G_{bulk} = 2\mu_{\mathrm{Mo}} + \mu_{\mathrm{C}}$. This simplifies Equation (S6) to,

$$\gamma_{surf}(T,p) = \frac{1}{2A}\left(G_{slab} - \frac{N_{\mathrm{Mo}}G_{bulk}}{2} + \frac{N_{\mathrm{Mo}} - 2N_{\mathrm{C}}}{2}\mu_{\mathrm{C}}\right) \qquad (S7)$$

In the presence of hydrogen, the surface energy can be written as,

$$\gamma_{surf}^{\mathrm{H}_2}(T,p) = \frac{1}{2A}\left(G_{slab} - N_{\mathrm{Mo}}\mu_{\mathrm{Mo}} - N_{\mathrm{C}}\mu_{\mathrm{C}} - N_{\mathrm{H}_2}\mu_{\mathrm{H}_2}\right) \qquad (S9)$$

where we use $\mu_{\mathrm{H}_2} = G_{\mathrm{H}_2}$, and can be simplified as

$$\gamma_{surf}^{\mathrm{H}_2}(T,p) = \gamma_{surf}(T,p_i) + \frac{1}{2A}(n\Delta G_{\mathrm{H}^*}) \qquad (S10)$$

The bonding properties

The bond properties between adsorbed hydrogen and surface atoms are inspected by binding distances which are inversely proportional to binding energy of hydrogen on surfaces; namely, stronger bonding is associated with shorter bonding distances. In Table S4, the C-H bond, which is formed at C related sites, is shorter than the Mo-H bond formed at Mo related sites (the bond enthalpies for C-H and Mo-H are 338.4 and 202 kJ/mol, respectively). Accompanied with the charge analysis shown in the same Table S4, there are more charge transfers between Mo-H bonds than C-H bonds, which shows the metallic M-H and covalent C-H bond properties.

Table S5. The Hydrogen adsorption energies with zero-point energy correction (in eV), binding distance (in Å) and charge of H (in e) on high symmetry sites, which are indicated by the three numbers from left to right.

(011)		(101)		(110)		(021)		(111)-Mo	
C_1	-0.51/1.12/0.90	B_1	-0.95/1.89/1.41	B_1	-0.99/1.90/1.41	OB_1/OB_2	-0.94/1.95/1.46	B_1	-0.95/1.92/1.41
C_2	-0.51/1.12/0.90	B_2	-0.63/1.93/1.36	B_2	-0.99/1.90/1.41	H_9/H_{10}	-0.86/1.93/1.44	B_3	-0.87/1.89/1.43
OB_3	-0.21/1.91/1.30	E_3	-0.49/1.94/1.37	B_3	-0.66/1.93/1.40	B_3/B_4	-0.78/1.88/1.41	E_2	-0.85/1.95/1.41
OB_4	-0.21/1.91/1.30	C_4	-0.48/1.12/0.90	B_4	-0.66/1.93/1.40	B_5/B_6	-0.76/1.94/1.41	E_7	-0.74/1.90/1.42
		OB_5	-0.24/1.84/1.32	C_5	-0.41/1.13/0.95	H_7/H_8	-0.58/2.07/1.41	E_8	-0.66/1.95/1.40
				C_6	-0.41/1.13/0.95			B_4	-0.59/1.95/1.40

(100)-C		(100)-Mo		(001)-C		(001)-Mo		(010)-Mo	
C_1	-0.89/1.10/0.84	H_1	-0.93/1.97/1.44	C_1	-0.51/1.10/0.87	H_1	-1.06/1.96/1.46	OB_1	-0.94/1.95/1.43
C_2	-0.89/1.10/0.84	H_2	-0.93/1.97/1.44	C_4	-0.51/1.10/0.87	H_2	-1.06/1.96/1.46	OB_2	-0.94/1.95/1.43
H_3	-0.16/1.85/1.25	H_3	-0.89/1.94/1.44	H_2	-0.38/1.99/1.34	H_3	-0.97/2.02/1.43	E_3	-0.52/1.86/1.33
H_4	-0.16/1.85/1.25	H_4	-0.89/1.94/1.44	H_3	-0.38/1.99/1.34	H_4	-1.01/2.02/1.44	E_4	-0.52/1.86/1.33
		H_5	-0.79/1.97/1.39						
		H_6	-0.79/1.97/1.39						

The Exchange Current Densities Analysis

Table S6. Exchange current densities of β-Mo_2C NPs collected from experiments

J_0 (A/cm^{-2})	Electrolyte	Synthesis Method
1.729 e-5[7]	0.1 M HClO4	Solution route
2.683 e-6 / 1.037[8] e-5	0.5M H_2SO_4 / 1M KOH	Urea glass route
1.3 e-6 / 3.8 e-6[9]	1M H_2SO_4 / 1M KOH	Commercial NPs
3.3 e-5[10]	0.5M H_2SO_4	Solution route
7.94e-7[11]	0.5M H_2SO_4	carburization with CH4
7.38e-7[12]	1 M KOH	commercial
1.95e-6/3.43e-5[13] (commercial./synthesized though solution route)	0.5M H_2SO_4	Solution route
4.0e-5[14]	0.05MH2SO4	mpg-C3N4 a
4.22e-6[15]	0.5M H_2SO_4	Solution route
3.79e-6[16]	0.5M H_2SO_4	Solution route
3.80e-6[17]	0.5M H_2SO_4	Solution route
7.9e-7[18]	0.5M H_2SO_4	MoO4 H_2O

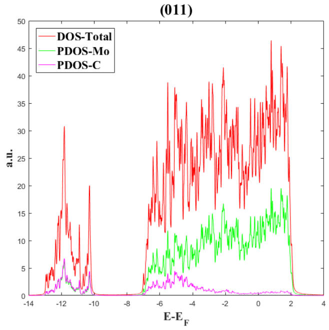

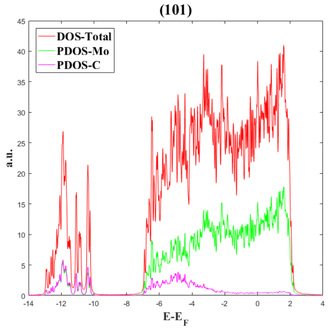

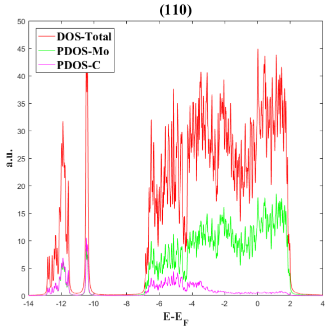

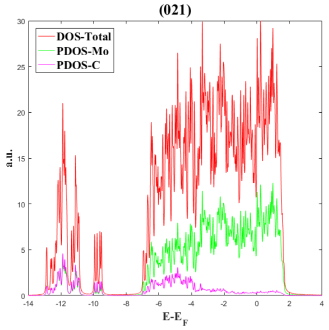

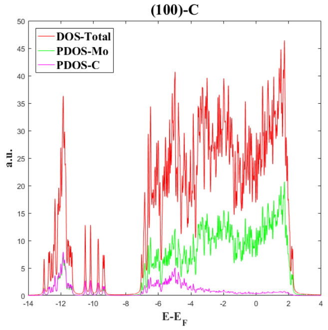

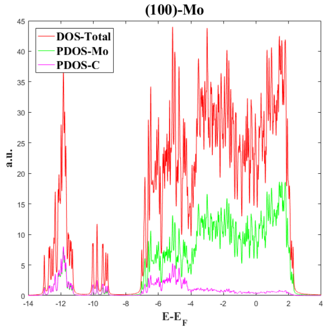

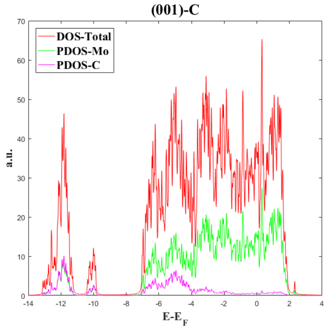

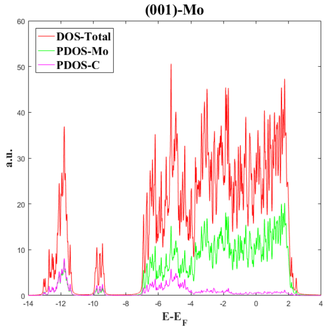

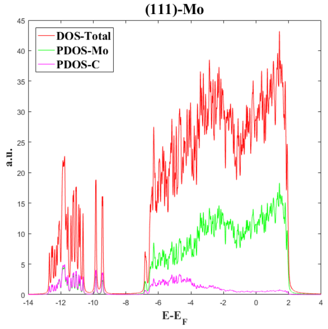

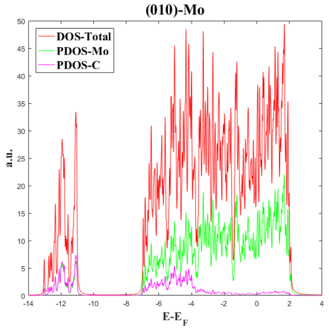

Table S7. The density of states of the ten β-Mo_2C surfaces.

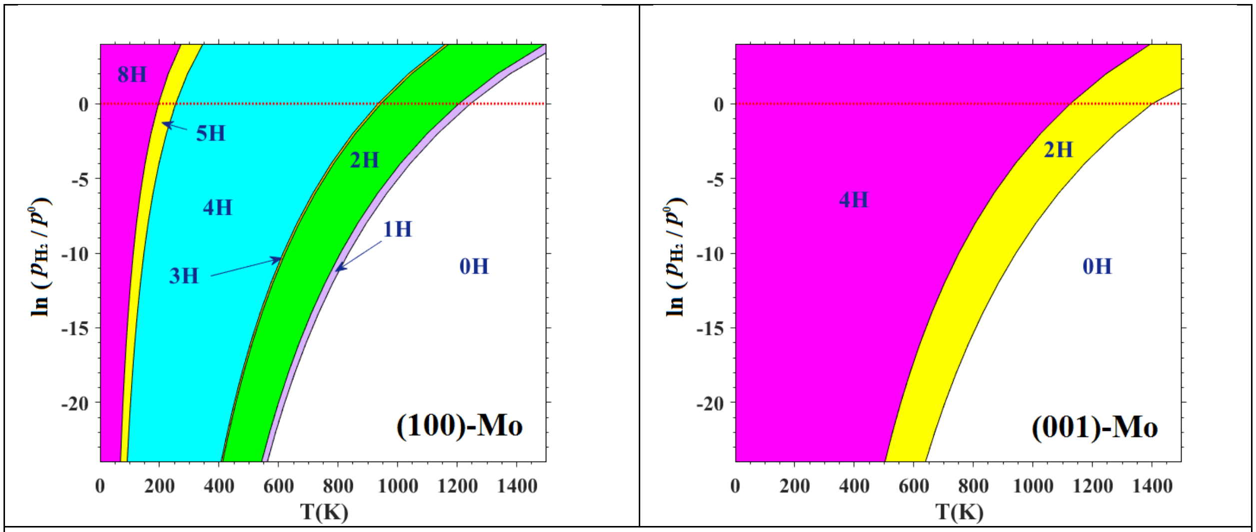

Table S8. The Hydrogen composition phase diagram of (100)-Mo and (001)-Mo surface

Table S9.

	hydrogen gas environment log(j)	Vacuum Log(j)
NP$_{-6}$	-4.91	-4.63
NP$_{-7}$	-4.83	-4.54
NP$_{-8}$	-4.79	-4.50
NP$_{-9}$	-4.77	-4.47
NP$_{-10}$	-8.09	-7.72
NP$_{-11}$	-8.30	-7.78

References

1 Blochl, P. E. Projector augmented-wave method. *Phys Rev B* **50**, 17953-17979, doi:DOI 10.1103/PhysRevB.50.17953 (1994).

2 Kresse, G. & Joubert, D. From ultrasoft pseudopotentials to the projector augmented-wave method. *Phys Rev B* **59**, 1758-1775, doi:DOI 10.1103/PhysRevB.59.1758 (1999).

3 Shi, X.-R. *et al.* Structure and stability of β-Mo2C bulk and surfaces: A density functional theory study. *Surface Science* **603**, 852-859, doi:10.1016/j.susc.2009.01.041 (2009).

4 Chen, Y. *et al.* Facile Synthesis and Thermal Stability of Nanocrystalline Molybdenum Carbide. *Materials Sciences and Applications* **02**, 1313-1316, doi:10.4236/msa.2011.29178 (2011).

5 Wang, T., Li, Y.-W., Wang, J., Beller, M. & Jiao, H. Dissociative Hydrogen Adsorption on the Hexagonal Mo2C Phase at High Coverage. *The Journal of Physical Chemistry C* **118**, 8079-8089, doi:10.1021/jp501471u (2014).

6 Chase, M. W. *et al.* JANAF Thermochemical Tables, 1982 Supplement. *Journal of Physical and Chemical Reference Data* **11**, 695, doi:10.1063/1.555666 (1982).

7 Wan, C., Regmi, Y. N. & Leonard, B. M. Multiple phases of molybdenum carbide as electrocatalysts for the hydrogen evolution reaction. *Angew Chem Int Ed Engl* **53**, 6407-6410, doi:10.1002/anie.201402998 (2014).

8 Ma, L., Ting, L. R. L., Molinari, V., Giordano, C. & Yeo, B. S. Efficient hydrogen evolution reaction catalyzed by molybdenum carbide and molybdenum nitride nanocatalysts synthesized via the urea glass route. *J. Mater. Chem. A* **3**, 8361-8368, doi:10.1039/c5ta00139k (2015).

9 Heron Vrubel, X. H. Molybdenum Boride and Carbide Catalyze Hydrogen Evolution inboth Acidic and Basic Solutions. *Angewandte Chemie* **51**, 12703-12706 (2012).

10 Tang, C., Sun, A., Xu, Y., Wu, Z. & Wang, D. High specific surface area Mo2C nanoparticles as an efficient electrocatalyst for hydrogen evolution. *Journal of Power Sources* **296**, 18-22, doi:10.1016/j.jpowsour.2015.07.016 (2015).

11 Kelly, T. G., Lee, K. X. & Chen, J. G. Pt-modified molybdenum carbide for the hydrogen evolution reaction: From model surfaces to powder electrocatalysts. *Journal of Power Sources* **271**, 76-81, doi:10.1016/j.jpowsour.2014.07.179 (2014).

12 Wu, Z.-Y. *et al.* Mo2C nanoparticles embedded within bacterial cellulose-derived 3D N-doped carbon nanofiber networks for efficient hydrogen evolution. *NPG Asia Materials* **8**, e288, doi:10.1038/am.2016.87 (2016).

13 Mu, Y. *et al.* Controllable synthesis of molybdenum carbide nanoparticles embedded in porous graphitized carbon matrixes as efficient electrocatalyst for hydrogen evolution reaction. *Electrochimica Acta* **215**, 357-365, doi:10.1016/j.electacta.2016.08.104 (2016).

14 Alhajri, N. S., Anjum, D. H. & Takanabe, K. Molybdenum carbide–carbon nanocomposites synthesized from a reactive template for electrochemical hydrogen evolution. *Journal of Materials Chemistry A* **2**, 10548, doi:10.1039/c4ta00577e (2014).

15 Pan, L. F. *et al.* Molybdenum carbide stabilized on graphene with high electrocatalytic activity for hydrogen evolution reaction. *Chem Commun (Camb)* **50**, 13135-13137, doi:10.1039/c4cc05698a (2014).

16 He, C. & Tao, J. Synthesis of nanostructured clean surface molybdenum carbides on graphene sheets as efficient and stable hydrogen evolution reaction catalysts. *Chem Commun (Camb)* **51**, 8323-8325, doi:10.1039/c5cc01240f (2015).

17 He, C. & Tao, J. Exploration of the electrochemical mechanism of ultrasmall multiple phases molybdenum carbides nanocrystals for hydrogen evolution reaction. *RSC Adv.* **6**, 9240-9246, doi:10.1039/c5ra25367e (2016).

18 Ang, H. *et al.* Hydrophilic Nitrogen and Sulfur Co-doped Molybdenum Carbide Nanosheets for Electrochemical Hydrogen Evolution. *Small* **11**, 6278-6284, doi:10.1002/smll.201502106 (2015).